Marine Pollution Bulletin 141 (2019) 91–103

Contents lists available at ScienceDirect

Marine Pollution Bulletin

journal homepage: www.elsevier.com/locate/marpolbul

Dilution characteristics of riverine input contaminants in the Seto Inland Sea

Junying Zhu[a,b,c], Xinyu Guo[a,b,*], Jie Shi[a,c], Huiwang Gao[a,c]

[a] Key laboratory of Marine Environment and Ecology, Ocean University of China, Ministry of Education, 238 Songling Road, Qingdao 266100, China
[b] Center for Marine Environmental Studies, Ehime University, 2-5 Bunkyo-Cho, Matsuyama 790-8577, Japan
[c] Laboratory for Marine Ecology and Environmental Sciences, Qingdao National Laboratory for Marine Science and Technology, Qingdao 266071, China

ARTICLE INFO

Keywords:
Dilution
Riverine pollution
The Seto Inland Sea
Hydrodynamic model
Residual currents

ABSTRACT

Riverine input is an important source of contaminants in the marine environments. Based on a hydrodynamic model, the dilution characteristics of riverine contaminants in the Seto Inland Sea and their controlling factors were studied. Results showed that contaminant concentration was high in summer and low in winter. Contaminant concentration decreased with the reduction of its half-life period, and the relationship between them followed power functions. Sensitivity experiments suggested that the horizontal current and vertical stratification associated with air-sea heat flux controlled the seasonal cycle of contaminant concentration in the water column; however, surface wind velocity was the dominant factor affecting the surface contaminant concentration. In addition, contaminant concentration in a sub-region was likely controlled by the variations in river discharges close to the sub-region. These results are helpful for predicting contaminant concentrations in the sea and are expected to contribute to assessing the potential ecological risks to aquatic organisms.

1. Introduction

With the rapid development of human life, more and more terrestrial chemical substances, such as pharmaceuticals (Hirsch et al., 1999; Managaki et al., 2007), polychlorinated biphenyls (Burreau et al., 2006), polycyclic aromatic hydrocarbons (Montuori and Triassi, 2012) and organochlorine pesticides (Hu et al., 2009), enter the natural water environment and are detected in coastal seas around the world. The adverse ecological risks of these contaminants to aquatic organisms are a major concern due to their potential toxic effects and biomagnification in marine mammals (Halling-Sørensen et al., 1998; Burreau et al., 2006).

Among these contaminants, persistent organic pollutants (POPs) have been of concern over the last decade (Iwata et al., 1993; Lohmann et al., 2006) because they have a long half-life period and remain in water environments for years. On the other hand, some contaminants, such as antibiotics, have a short half-life period of a few days and are relatively easy to remove from water environments. However, due to the potential threat to ecosystem balance and risk to health of humans and animals, antibiotics in aquatic environments have generated growing interest among researchers in recent years (Marti et al., 2014; Chow et al., 2015; Grill et al., 2016; Liu et al., 2017; Liu et al., 2018). Antibiotics that enter water environments exert constant selection pressure on both bacterial fish pathogens and marine microbial populations, increasing the emergence of antibiotic resistant strains (Boon and Cattanach, 1999; Vivekanandhan et al., 2002; Baquero et al., 2008) and severely damaging fisheries production (Karunasagar et al., 1994; Majtán et al., 2012). Previous studies have concluded that most antibiotics pose a relatively high ecological risk to relevant aquatic organisms in marine environments (Lee et al., 2008; Zhao et al., 2010; Zhang et al., 2012). Moreover, the degree of the effect of these contaminants on aquatic organisms mainly depends on their concentration in the water.

Riverine input is a major source of contaminants in marine environment and a high concentration of contaminants in rivers has been observed in many countries (Xu et al., 2007; Minh et al., 2009; Zhao et al., 2010; da Silva et al., 2011; Zou et al., 2011; Zhang et al., 2012; Grill et al., 2016). However, the contaminant concentrations in rivers and sea water are extremely different due to different hydrodynamic environments. When contaminants enter coastal seas from rivers, two major questions are raised. The first is whether the ocean dilutes the contaminant levels to a lower concentration (i.e., to a nontoxic degree) without considerable consequences to aquatic organisms. The second is what are the key factors controlling contaminant concentration in the sea.

To answer these questions, many fixed-point observations of the contaminant concentrations and risk assessments based on contaminant concentrations have been conducted in some coastal seas (Gómez-

* Corresponding author at: Center for Marine Environmental Studies, Ehime University, 2-5 Bunkyo-Cho, Matsuyama 790-8577, Japan.
E-mail address: guoxinyu@sci.ehime-u.ac.jp (X. Guo).

https://doi.org/10.1016/j.marpolbul.2019.02.029
Received 14 November 2018; Received in revised form 13 February 2019; Accepted 13 February 2019

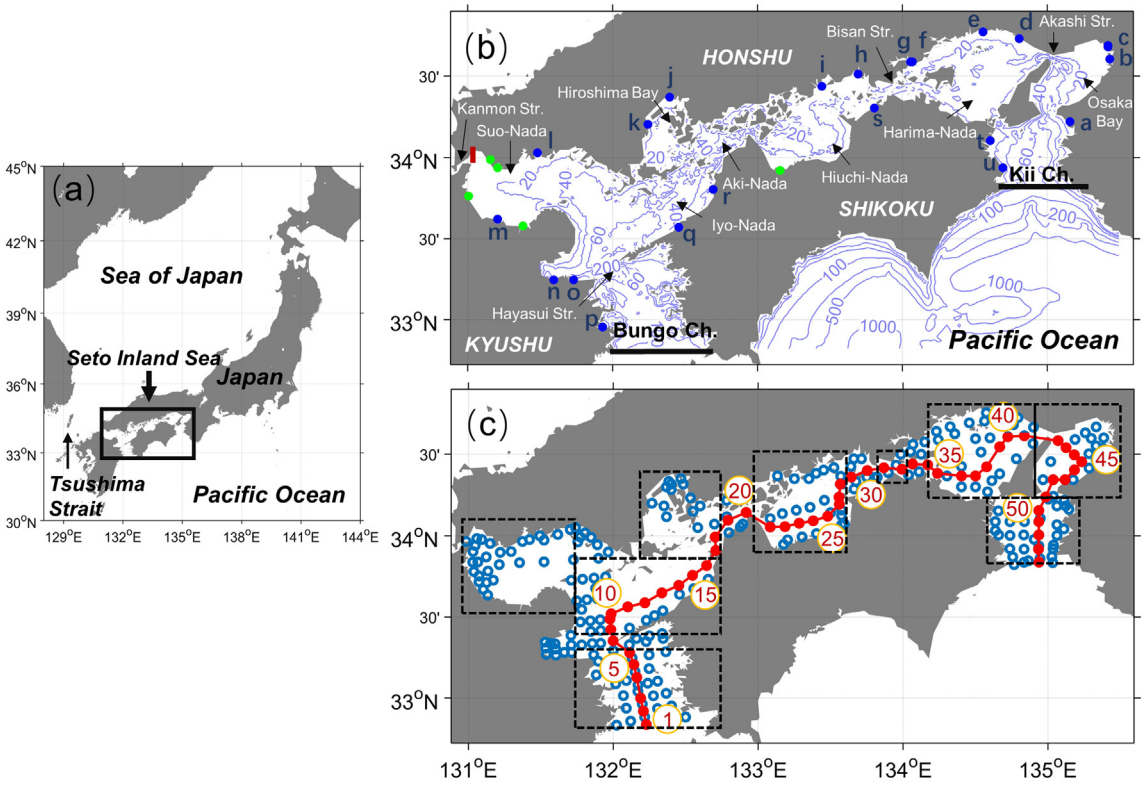

Fig. 1. (a) Location of the Seto Inland Sea (SIS). (b) Bathymetry (m) of the SIS and model domain. The solid black lines in (b) indicate the Bungo Channel and Kii Channel, which are the southern boundaries of the hydrodynamic model. The red solid line running in a northwest direction in (b) is the Kanmon Strait, which is closed in the model. The blue solid circles with lower case letters a to u along the coast in (b) are the locations of 21 major rivers (Table 1), and the green solid circles are the locations of the five secondary rivers. (c) Monthly observation stations in the SIS. The hollow blue circles and solid red circles in (c) are the monthly sampling stations. The solid red circles and lines with numbers from 1 to 50 denote selected stations to validate the model results in the vertical direction used in Fig. 4. The dashed black rectangles in (c) represent selected sub-regions for the purpose to show the seasonal variation of mean contaminant concentration in the sub-region. (For interpretation of the references to colour in this figure legend, the reader is referred to the web version of this article.)

Gutiérrez et al., 2007; Zhao et al., 2010). Two related factors were proposed. Dilution factors, defined as the concentration ratio of contaminants in a river (or effluent) and sea water near the outfalls, have been used to represent the dilution levels of sea water (Minh et al., 2009; Zhang et al., 2012). The other is the contaminant flux from rivers, which is the product of contaminant concentrations and river discharge, and it is often used to estimate the contribution of rivers to contaminant concentration in sea water (Wolschke et al., 2011; Zou et al., 2011; Montuori and Triassi, 2012). However, the key factors responsible for contaminant concentration in the ocean were still unclear, and it should be explored in a specific estuary or coastal sea.

Due to limitation in observation, there is insufficient data to show continuous spatio-temporal variation of contaminant concentration in sea water. In addition, previous dilution studies about contaminants have mostly focused on the areas around the mouths of rivers; therefore, there is a lack of information on dilution characteristics in offshore and shelf areas. Modeling is a powerful tool for coupling processes under different disciplines and spatio-temporal scales. To address these issues, a hydrodynamic model is required.

The Seto Inland Sea (SIS) region (Fig. 1) is one of the most industrialized areas in Japan. Murata et al. (2011) reported the results of a nationwide survey of commonly used human and veterinary antibiotics in 37 Japanese rivers. They found that concentrations of the sum of 12 target antibiotics in 8 rivers, which directly emptied into the SIS, ranged from low ng/L to 60 ng/L. The SIS is a major fishing ground (Nagai, 2003) that includes aquacultures sites for fish, bivalves, and seaweed; therefore, it is necessary to evaluate the dilution levels of antibiotics in the whole SIS.

The aim of this study was to investigate the dilution characteristics of riverine contaminants in the entire SIS and their influencing factors by using a hydrodynamic model. We first explored the spatial and temporal variations of concentrations of conservative contaminant and non-conservative contaminants (using antibiotics as an example), and then investigated the mechanisms controlling contaminant concentration in the SIS.

2. Model configuration and validation

2.1. Simulation and validation of temperature and salinity

The SIS is a shallow semi-enclosed shelf sea located in western Japan, with a surface area of 23,000 km^2 and an average depth of 38 m (Fig. 1a). It opens to the Pacific Ocean via the Bungo Channel and Kii Channel, through which tidal waves enter the SIS. It is surrounded by the islands of Honshu, Shikoku, and Kyushu, which are rapidly developing, urbanized regions in Japan. There are 21 first-order rivers and 643 secondary order rivers emptying into the SIS. It has a complicated geographical character, including a series of broad basins (called “nada” in Japanese), such as Suo-Nada, Iyo-Nada, Hiuchi-Nada, and Harima-Nada, which are connected to each other through narrow straits. The predominant tidal constituent in the SIS is the lunar semi-diurnal M_2 (Yanagi, 1981). Tidal currents are strong in the narrow straits (> 1 m/s) and weak in the broad basins (approximately 0.1 m/s) (Takeoka, 2002).

Appendix A describes the details of hydrodynamic model. Model domain ranges from 130.98°E to 135.5°E and from 32.8°N to 34.8°N (Fig. 1b). The model includes 21 major rivers and 5 secondary rivers whose locations along the coastline are shown in Fig. 1b. Multi-year

Table 1
Annual mean river discharges ($m^3 s^{-1}$) of 21 major rivers in the Seto Inland Sea, based on dataset of the Ministry of Land, Infrastructure and Transport. The locations of the rivers are shown in Fig. 1b.

No.	River	1994	Multi-year average (1993–2016)	2015
a	Kino	30.74	48.47	35.05
b	Yamato	13.51	25.62	28.52
c	Yodo	151.44	261.65	308.14
d	Kako	17.53	57.82	409.89
e	Ibo	17.52	27.20	36.28
f	Yoshii	34.2	58.81	70.11
g	Asahi	30	52.63	57.39
h	Takahashi	31.19	52.17	8.76
i	Ashida	3.93	11.20	13.56
j	Oota	13.46	57.78	72.18
k	Oze	8.42	12.63	13.65
l	Saba	10.85	17.20	18.3
m	Yamakuni	7.4	21.03	21.56
n	Oita	13.58	26.21	25.84
o	Oono	33.08	60.35	48.43
p	Bansho	4.05	12.56	8.28
q	Hiji	4.96	29.11	42.73
r	Sigenobu	4.23	9.65	12.54
s	Doki	1.07	2.13	2.18
t	Yoshino	40.7	39.90	35.72
u	Naka	43.03	66.66	80.13

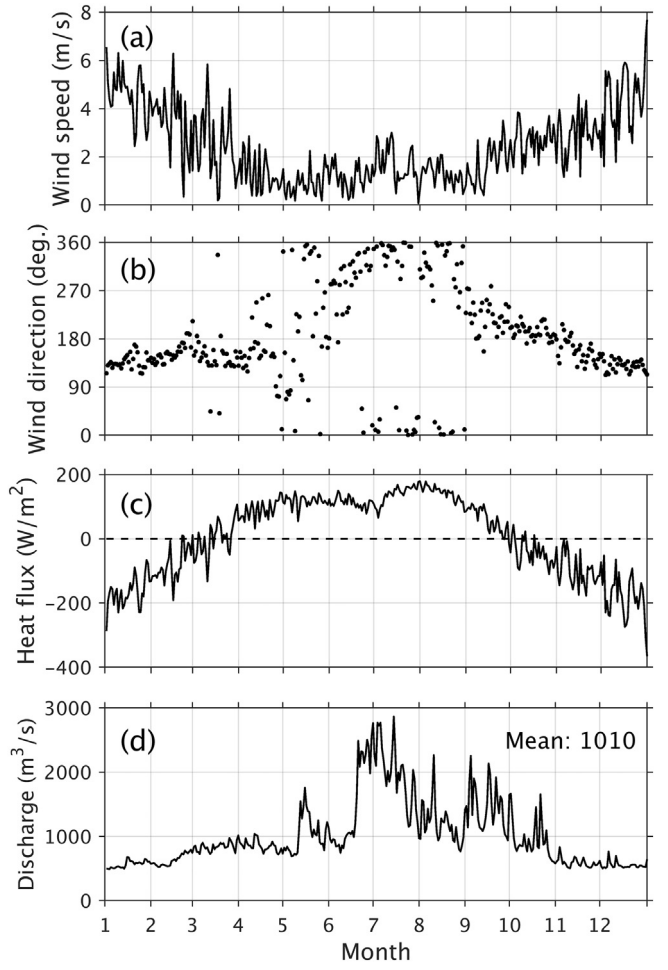

Fig. 2. Daily variations in multi-year averaged (a) wind speed, (b) wind direction, (c) air-sea heat flux, and (d) river discharges used in case Control. The wind direction in (b) is clockwise and the direction of southerly wind is 0. Positive values in (c) indicate that the ocean gains heat, while negative values indicate the opposite situation.

averaged river discharges are used (discharges of the 21 major rivers were shown in Table 1). Compared with the major rivers, the discharges of the five secondary rivers are much smaller with a total annual mean discharge of 61 $m^3 s^{-1}$. In terms of the seasonal variation, the discharge of 26 major and secondary rivers reaches its maximum (2868 $m^3 s^{-1}$) in July and minimum (490 $m^3 s^{-1}$) in January, with a mean value of 1010 $m^3 s^{-1}$ (Fig. 2d).

In addition to river discharge, the model was also driven by climatological atmospheric forcing (wind stresses and air-sea heat flux, Fig. 2). It started with an initial condition in January and run for three years to finish its spin-up. The results in the fourth year were used in the present study. The temperature, salinity, and current velocity were saved at 1-hour interval, and the impacts of tides were removed by applying a tide filter (Hanawa and Mitsudera, 1985) to the hourly saved results. Regular hydrographic observations at monthly intervals have been carried out over the past 40 years by prefectural fishery research centers around the SIS and the locations of the observation stations are shown in Fig. 1c. The observed temperature and salinity data from 1972 to 2000 at standard levels were obtained and used to validate model results. February and July are used to represent winter and summer, respectively.

In winter, warm and saline waters flowed into the SIS through the Bungo Channel and Kii Channel. Consistent with the observations, the sea surface temperature reached 16 °C and 14 °C in the Bungo Channel and Kii Channel (Fig. 3a, b), respectively. The surface salinity in the Bungo Channel was 34–34.5, which was larger than that of around 33.5 in the Kii Channel (Fig. 3e, f). Both temperature and salinity became lower toward the middle of the SIS. In terms of vertical distributions (Fig. 4), both observation and model results showed that the water column was well-mixed throughout the entire SIS (Fig. 4a-b, e-f). Temperature was low around stations 25–40 with values of around 8–9 °C. Low salinity water occurred around station 45 in Osaka Bay because of the large discharge from the Yoda River (Table 1).

In summer, sea surface temperature was as high as 21–25 °C. Low temperature waters of about 21 °C occurred around the Hayasui Strait and Aki-Nada (Fig. 3c, d). The salinity showed low values (< 30) around the mouths of river and high values in the Bungo Channel (33–34) and Kii Channel (31.5–32.5) (Fig. 3g, h). Both temperature and salinity exhibited a well-mixed pattern around the straits (stations 19–20 and 30–32) and a well-stratified in the broad basins (stations 10–15, 22–28, 35–40) (Fig. 4c–d, g–h). Similar to the observations, warm surface pools and cold bottom water were established in Iyo-Nada (stations 10–15) and Harima-Nada (stations 35–40), although the bottom water temperature in Harima-Nada was 3 °C lower in the model than in the observation (Fig. 3c, d). Low salinity waters existed in Osaka Bay (stations 40–50), forming a front structure with high salinity water in the Kii Channel (Fig. 4g, h).

The simulated temperature and salinity were climatological patterns since the hydrodynamic model was driven by the multi-year mean forcings (wind stresses, river discharge and heat flux). On the other hand, the observations were carried out at fixed-stations on a specified day and their monthly mean was the averaged value of snapshot observations in the same month over many years. Considering the nonlinear system of ocean and the difference in sample numbers for averaging between observations and model results, it is difficult to expect a perfect agreement between observation and model results. The correlation coefficients of temperature and salinity between observation and model results were 0.98 and 0.79 ($p < 0.01$) throughout a year. In general, the seasonal variations in temperature and salinity are well reproduced by the model (Figs. 3 and 4), which in some senses demonstrates that the model can give generally accurate current fields. Therefore, the hydrodynamic model can be used to simulate the distribution of contaminant.

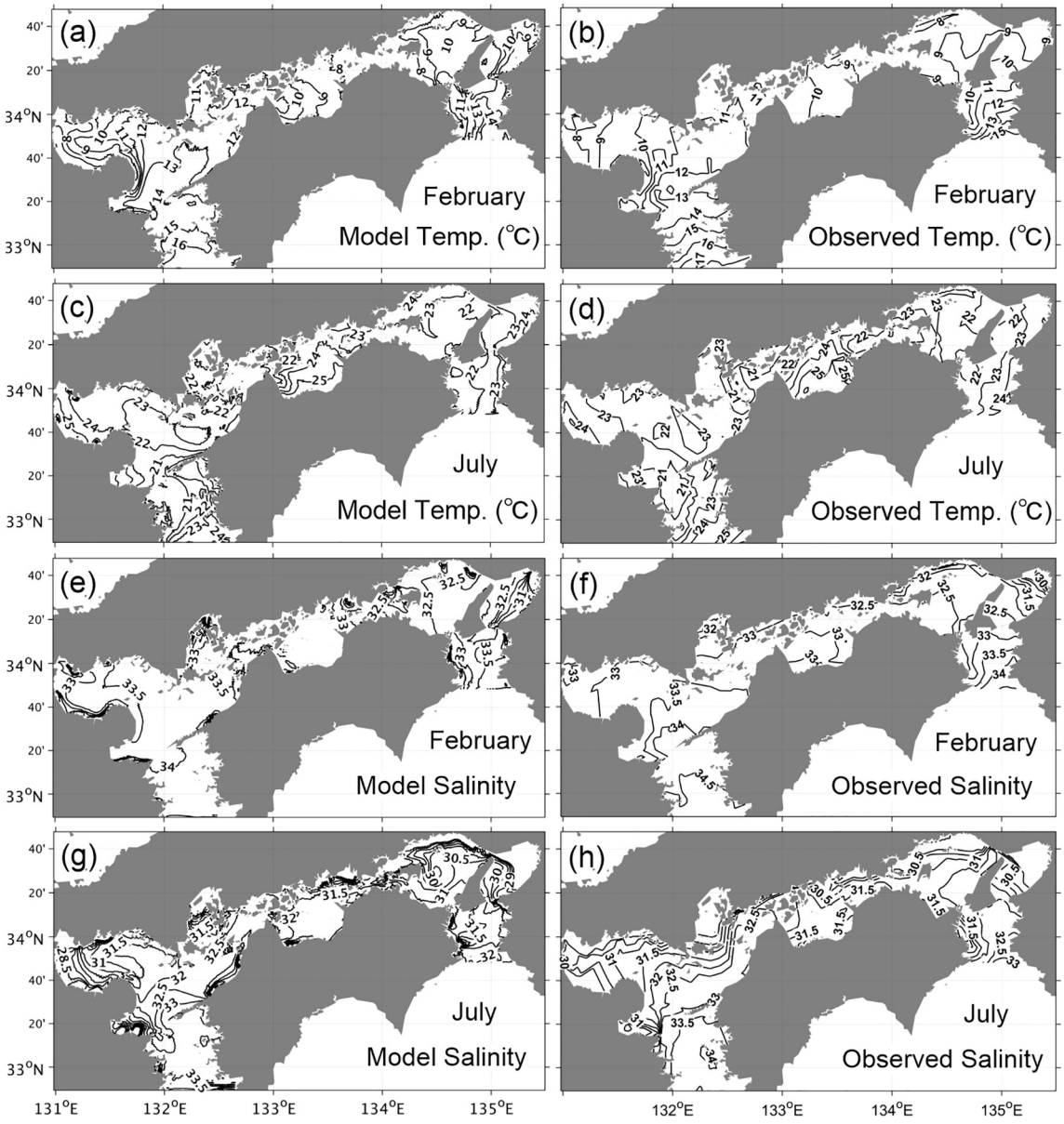

Fig. 3. Spatial distributions of simulated and observed (a-d) surface temperature and (e-h) salinity in February and July in the SIS.

2.2. Simulation of contaminant concentration

In this study, we investigated conservative and non-conservative contaminants discharged into the SIS from rivers. Conservative contaminants do not decay with time and are used to represent contaminants such as most POPs that have a half-life period of several years which is longer than the mean residual time (~15 months) of the total sea water in the SIS (Takeoka, 1984). On the other hand, non-conservative contaminants are considered to decay with a time scale shorter than the mean residual time (~15 months) of sea water in the SIS. Antibiotic is a typical non-conservative contaminant. Xu et al. (2009) suggested that the half-life periods of four commonly used antibiotics, ofloxacin (OFL), roxithromycin (RTM), erythromycin (ETM), and sulfamethoxazole (SMZ) were 3.4 days, 6.7 days, 7.3 days, and 14.7 days in the flume seawater system, respectively. Therefore, the conservative contaminants and the four antibiotics were selected as targets of simulation in this study.

The initial concentration of contaminant in the SIS and the concentration at two boundaries with open ocean (the Bungo Channel and Kii Channel) were set to 0. Contaminant was released from rivers and its concentration was set to 100. Since the contaminant concentration in the ocean had the same unit as the riverine contaminant concentration, we did not specify its unit in this study. In fact, it can be the unit of any concerned contaminant. Contaminants were controlled by the processes of advection, diffusion, and attenuation (only non-conservative contaminants) in the model. The attenuation of non-conservative contaminant was described in Appendix B for details.

The number of grids in the model is $362(x) \times 238(y) \times 21(z)$, where x is zonal direction, y is meridional direction and z is vertical direction (see Appendix A). Along with the hydrodynamic model online, the contaminant concentration defined in the center of each grid point was calculated at a time step of 120 s. The averaged contaminant concentration within one day was saved at 1-day interval during the model calculation. Based on the concentration at each grid point, the volume-averaged concentration (C_v) in the SIS was calculated as follow.

$$C_v = \frac{\int_1^{IM}\int_1^{JM}\int_1^{20} C(i,j,k)\,dzdydx}{\int_1^{IM}\int_1^{JM}\int_1^{20} dzdydx}$$

i, j, k are grid indexes along the x, y, z directions, respectively. IM

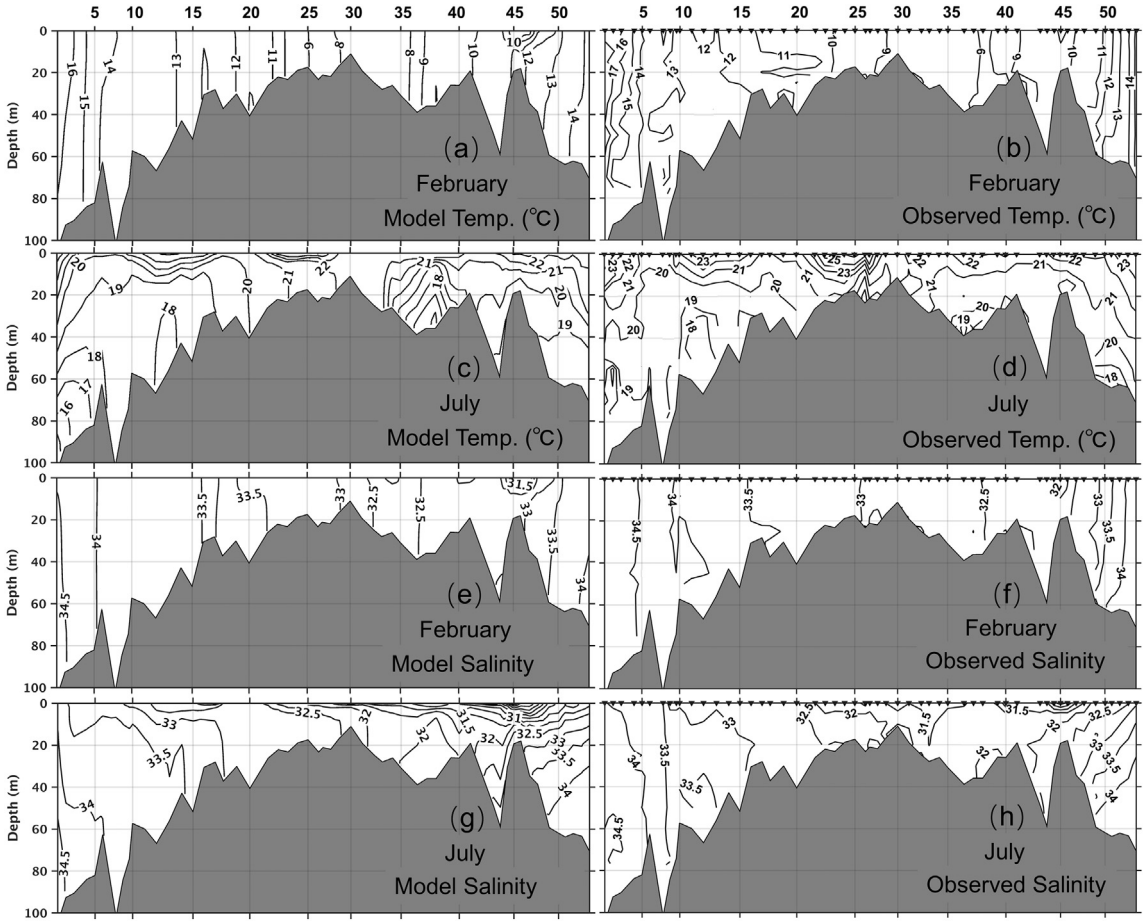

Fig. 4. The same as Fig. 3, but for vertical distributions along the solid red line with numbers in Fig. 1c. The numbers of stations correspond to numbers from 1 to 50 in Fig. 1c. (For interpretation of the references to colour in this figure legend, the reader is referred to the web version of this article.)

and *JM* are grid numbers in *x* and *y* directions. Apparently, C_v was an averaged concentration using weighting factor of volume of each grid point. Similarly, the area-averaged surface concentration (C_a) in the SIS was calculated as follow.

$$C_a = \frac{\int_1^{IM}\int_1^{JM} C(i,j,1)dydx}{\int_1^{IM}\int_1^{JM} dydx}$$

C_v and C_a were first calculated from daily saved model results and then were averaged for a month (=monthly mean) and a year (=annual mean). Several important sub-regions (rectangle in Fig. 1c) were selected for the purpose to know the seasonal variation of mean contaminant concentration inside the sub-regions where both C_a and C_v were also calculated.

3. Results

3.1. Spatio-temporal variations of conservative contaminants

This section investigated the temporal variations and spatial distributions of conservative contaminants originating from rivers in the SIS by case Control listed in Table 2. Fig. 5a showed the temporal variation of contaminant concentration in the entire SIS. The average concentration in the fourth year was almost the same as that in the third year. Therefore, we analyzed the results in the fourth year. The same applied to all numerical experiments listed in Table 2.

The annual mean of C_v in the entire SIS was 1.64, showing a high value of 2.03 in July and a low value of 1.39 in January (Fig. 5a). The annual mean of C_a was 4.03, which was more than twice the annual mean of C_v. Consequently, the dilution factor of conservative contaminants in the entire SIS was 61 for C_v and 25 for C_a. In different sub-regions, the contaminant concentrations showed apparent distinctions (Fig. 5b, c). For C_v, the high value occurred in Harima-Nada, Osaka Bay, and the Bisan Strait with an annual mean of 4.58, 3.87, and 3.84, respectively (Fig. 5b). The annual mean of C_v were 2.18, 1.97, and 1.86 in Hiuchi-Nada, Suo-Nada, and Hiroshima Bay (Fig. 5b), respectively. Low value of C_v was found in the Kii Channel, Iyo-Nada, and the Bungo Channel with an annual mean value of 1.57, 1.11, and 0.42, respectively (Fig. 5b).

River was the only source of contaminant in the SIS and the total input amount of pollutants were proportional to the river discharges because we used a constant contaminant concentration in the river water. There were two rivers around Osaka Bay: the Yamato River and Yodo River (Fig. 1b and Table 1). The river discharges of both were high in summer and low in winter, and the highest value occurred in July (figures not shown), which agreed with the seasonal variation of contaminant concentration in Osaka Bay (Fig. 5b, c). Besides, the annual mean discharge of Yodo River was 261.65 $m^3 s^{-1}$ while that of Yamato River was only 25.62 $m^3 s^{-1}$ (Table 1). Therefore, the Yodo River was responsible for the high concentration values and seasonal variation in Osaka Bay.

Four rivers (d, e, f, g in Fig. 1b and Table 1) emptied into Harima-Nada with a total discharge of 196.46 $m^3 s^{-1}$ (the Kako River and Ibo River emptied directly into the sub-region of Harima-Nada, while the Yoshii River and Asahi River did not directly empty into it), which was less than that of the Yodo River. However, the C_v in Harima-Nada was higher than that in Osaka Bay (Fig. 5b). By calculating water age of Yodo River's waters using constituent-oriented age and residence time

Table 2
List of numerical experiments.

No.	Case	River discharge	Concentration in river	Half-life period of contaminant (days)	Forcing
1	Control	Normal	100	×	Normal
2	OFL	Normal	100	3.4	Normal
3	RTM	Normal	100	6.7	Normal
4	ETM	Normal	100	7.3	Normal
5	SMZ	Normal	100	14.7	Normal
6	Constant-river	Annual mean ($1010\ m^3\ s^{-1}$)	100	×	Normal
7	No-wind	Normal	100	×	No wind forcing
8	Constant-heat	Normal	100	×	Annual mean air-sea heat flux field in Supplementary Fig. 2
9	River-1994	1994	100	×	Normal
10	River-2015	2015	100	×	Normal

Note: × indicates that the contaminant is conservative.

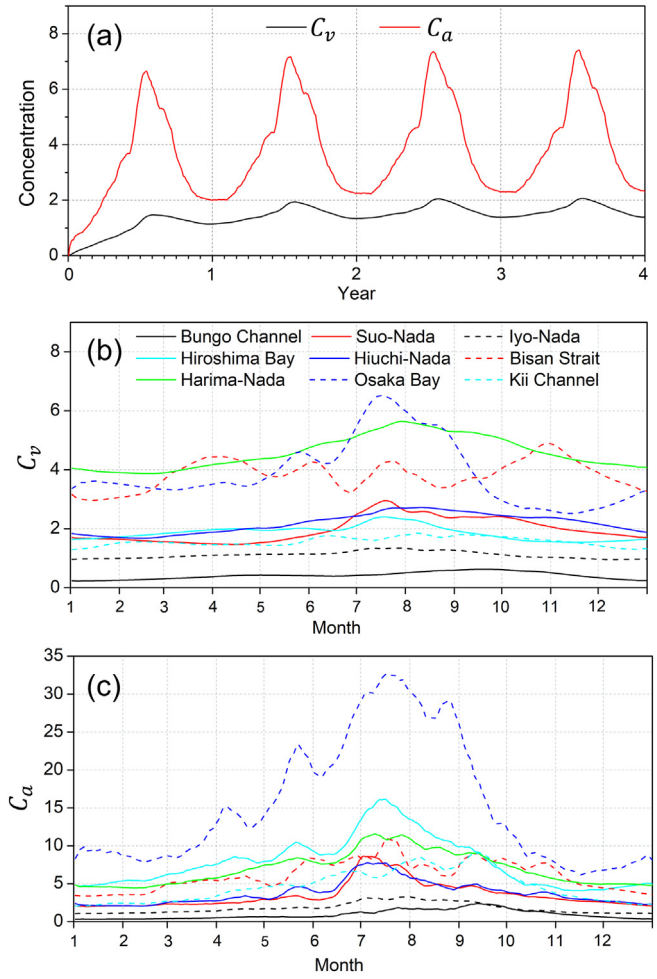

Fig. 5. Time series of (a) 15-day running mean of C_v and C_a over the entire SIS of case Control in four computational years. (b) and (c) are 7-day running mean of C_v and C_a in selected sub-regions in the fourth year, respectively.

theory, Wang et al. (2019) suggested that about 3/8 of the Yodo River's waters were brought into Harima-Nada though the Akashi Strait and eventually entered the Kii Channel. These waters were thought to have contributed to the high concentration values in Harima-Nada.

It was surprising that the C_v was high in the sub-region of the Bisan Strait (Fig. 5b) because no river directly emptied into this sub-region (Fig. 1b, c). Previous studies have determined that the tidal energy input from the Bungo Channel moved eastward along the main channels and encountered westward propagative tidal energy input from the Kii Channel in the Bisan Strait (Yanagi et al., 1982; Kobayashi et al., 2006). This indicated a weak dynamic exchange ability in the Bisan Strait that allowed the contaminants to be trapped there. The seasonal variation of contaminant concentration in the Bisan Strait was not likely related to river discharge, but rather the dynamic exchange ability with surrounding regions.

C_a showed a similar seasonal cycle as C_v over the entire SIS (Fig. 5a), which was consistent with seasonal variation in river discharges (Fig. 2d). For sub-regions, C_a in Osaka Bay was the largest with an annual mean of 15.38. The next was Hiroshima Bay and Harima-Nada with an annual mean of 7.82 and 6.96, respectively (Fig. 5c). The maximum value of C_a is larger in the eastern SIS than in the western SIS (Fig. 6a). It was over 30 in Osaka Bay, and over 15 in Hiroshima Bay, northern Harima-Nada, western Suo-Nada, and other river mouths (Fig. 6a). The maximum value of C_a occurred mostly in July (Fig. 6b). However, the occurrence times in the Bungo Channel and Kii Channel were close to August and September (Figs. 5c and 6b). The time lag of 1–2 months in the Bungo Channel and Kii Channel was caused by the contaminant transport from river mouths to the open ocean.

The vertical distributions of contaminant concentrations in four seasons were shown in Fig. 7. The concentration exhibited a vertically mixed pattern in winter and a vertically varying pattern in summer, which was similar to those of salinity (Fig. 4e–h). High contaminant concentrations (> 3) occurred at stations 30–45 (the Bisan Strait, Harima-Nada, and Osaka Bay) throughout the year. A vertically varying

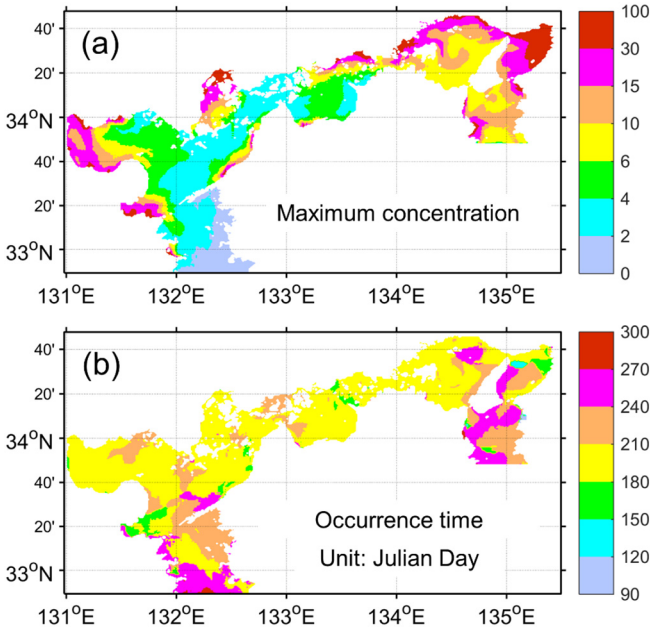

Fig. 6. Distributions of (a) maximum surface contaminant concentration and (b) its occurrence time in case Control.

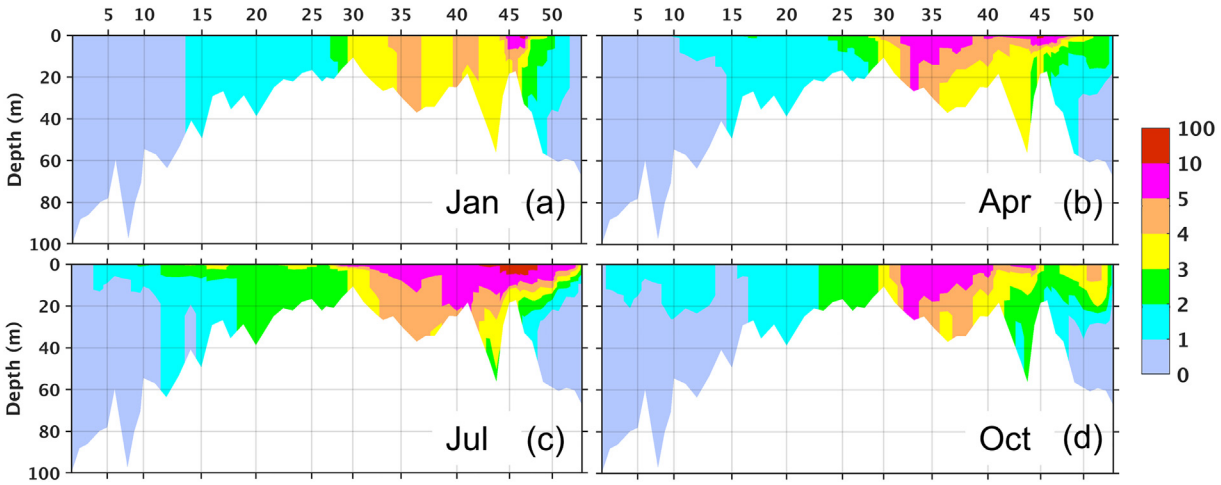

Fig. 7. Vertical distributions of contaminant concentrations in case Control along the solid red line with numbers in Fig. 1c in (a) January, (b) April, (c) July and (d) October. The numbers of stations correspond to numbers from 1 to 50 in Fig. 1c. (For interpretation of the references to colour in this figure legend, the reader is referred to the web version of this article.)

structure occurred from spring (April) to autumn (October), and reached its greatest variation in summer (July). Consequently, the C_a in Osaka Bay and Hiroshima Bay were 31.24 and 15.09 in July (Fig. 5c), which were around 5.0 and 6.5 times the C_v of 6.28 and 2.33 in the same sub-regions (Fig. 5b), respectively.

3.2. Dilution characteristics of non-conservative contaminants

Most riverine contaminants are non-conservative substances with a half-life period, which accelerates the removal efficiency of contaminants compared with conservative contaminants. Four experiments were run with half-life periods of four antibiotics, OFL, RTM, ETM, and SMZ, that represented non-conservative contaminants, and their experiments were named cases OFL, RTM, ETM, and SMZ, respectively (Table 2). Expect for half-life period of contaminant, the model configurations in the four experiments were the same as those in case Control. The results of the four antibiotic concentrations (figures not shown) presented the similar spatial distributions with the conservative contaminants (Fig. 6 and Fig. 7). However, the annual mean of C_v in the entire SIS were 0.36, 0.22, 0.21, and 0.12, while the annual mean of C_a were 2.16, 1.84, 1.80, and 1.52 for cases SMZ, ETM, RTM, and OFL, respectively. All these values were smaller than those of case Control (1.64 and 4.03, respectively).

As shown in Supplementary Fig. 1, no matter what the half-life period was, the concentrations exhibited coherent seasonal variations with case Control (Fig. 5). With an increase in the half-life period of contaminants, both C_v and C_a exhibited a prominent increase (Fig. 8a, b), which indicated that fewer contaminants decayed and more contaminants remained in the SIS. Furthermore, using a riverine input contaminant concentration of 100 as a reference, the relationship between concentration and half-life period of non-conservative contaminant could be depicted by the series of power functions listed in Table 3, which were within the 95% confidence interval and had r^2 values over 0.98. These functions made it possible to predict the contaminant concentration based on riverine input contaminant concentration and its half-life period, which contributed to assessing the risk to aquatic organisms. However, it should be noted that these relationships between concentration and half-life period were not applicable to conservative contaminants as well as non-conservative contaminants with half-life periods close to zero. Strictly speaking, the functions listed in Table 3 were credible when the half-life period ranged from 3.4 days to 14.7 days which were used as low limitation and high limitation of half-life period in our numerical experiments.

The vertical distributions of the four antibiotics also showed a vertically varying structure, especially in summer (figures not shown). The ratio of annual mean C_a to C_v might reveal the vertical variation and a large ratio indicated a strong vertical variation. As shown in Fig. 8c, in all the cases, the vertical variation of contaminants in the Bisan Strait was the weakest, while it was strong in Hiroshima Bay, Osaka Bay, and Hiuchi-Nada. As the half-life period of contaminants shortened, the ratio of annual mean C_a to C_v increased (Fig. 8c), which indicated that the vertical variation was enhanced. This meant that, under the same hydrodynamic conditions, contaminants with shorter half-life period tended to distribute in the surface layer because more contaminants decayed in the surface layer rather than entering the deep water.

4. Discussion

4.1. Key factors responsible for seasonal dilution of contaminant

In this section, the key factors responsible for seasonal dilution of contaminant were explored by performing three sensitivity experiments named cases Constant-river, No-wind, and Constant-heat (Table 2). The sea surface wind forcing was not included in case No-wind. The annual mean river discharge of each river was used in case Constant-river. The annual mean air-sea heat flux (Supplementary Fig. 2) was used throughout a year in case Constant-heat. Except for these specified conditions, the other model configurations in the three sensitivity experiments were the same as case Control. We compared C_v and C_a in the three sensitivity experiments with those in case Control (Fig. 9) and discussed the mechanisms in more detail below.

4.1.1. The role of sea surface wind forcing

When sea surface wind forcing was excluded, seasonal variations of both C_v and C_a showed similar patterns as those in case Control (black lines and green lines in Fig. 9a, c), but the contaminant concentration values were different (black lines and green lines in Fig. 9b, d). C_v in case No-wind was about 5% higher from December to June and 9% lower from July to November than that in case Control (Fig. 9a, b), while C_a in case No-wind was always higher (around 31%) than that in case Control (Fig. 9c, d).

The seasonal variations of meridional component of sub-tidal surface current velocity over the entire SIS in case Control and case No-wind can be found in Fig. 10. In winter, the surface southward current was stronger in case Control (4.2 cm/s) than in case No-wind (0.7 cm/s) (black and green dots in Fig. 10), indicating a southward wind-induced surface current of 3.5 cm/s. The southward surface current induced by

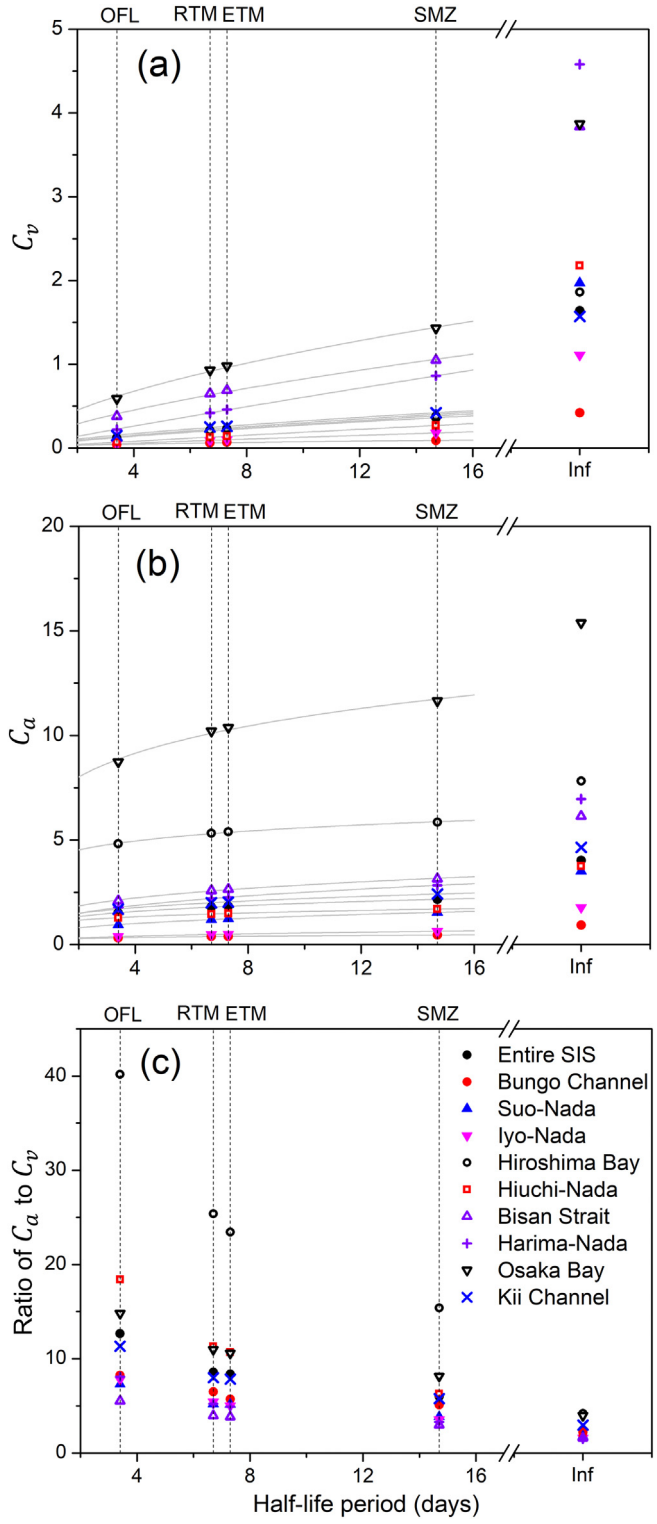

Fig. 8. The relationships between the half-life periods of contaminants and (a) C_v, (b) C_a, and (c) the ratio of C_a to C_v in several sub-regions of the SIS. Conservative contaminants are marked with "Inf". The gray solid lines in (a) and (b) represent the fitted curves according to functions in Table 3. OFL: ofloxacin, RTH: roxithromycin, ETM: erythromycin, SMZ: sulfamethoxazole.

northerly wind (Fig. 2b) facilitated the contaminant transport to the open ocean, decreasing the contaminant concentration (C_a and C_v) in case Control (Fig. 9a). In summer, a southerly wind in case Control (Fig. 2b) induced northward surface current, hindered the contaminant transport to the open ocean, and increased C_v as found in case Control (Fig. 9a).

Table 3
The fitted power functions of C_v and C_a (y) with half-life period of contaminant (x) shown in Fig. 8.

	C_v	C_a
Entire SIS	$y = 0.0519\ x^{0.7222}$	$y = 1.141\ x^{0.2384}$
Bungo Channel	$y = 0.0230\ x^{0.5142}$	$y = 0.2538x^{0.2234}$
Suo-Nada	$y = 0.0548\ x^{0.7412}$	$y = 0.6432\ x^{0.3262}$
Iyo-Nada	$y = 0.0175\ x^{0.8679}$	$y = 0.2562\ x^{0.3399}$
Hiroshima Bay	$y = 0.0493\ x^{0.7617}$	$y = 4.134\ x^{0.1308}$
Hiuchi-Nada	$y = 0.0222\ x^{0.9291}$	$y = 1.028\ x^{0.1877}$
Bisan Strait	$y = 0.1832\ x^{0.6532}$	$y = 1.531\ x^{0.271}$
Harima-Nada	$y = 0.0737\ x^{0.9149}$	$y = 1.198\ x^{0.3206}$
Osaka Bay	$y = 0.3036\ x^{0.5796}$	$y = 7.013\ x^{0.1918}$
Kii Channel	$y = 0.0663\ x^{0.688}$	$y = 1.264\ x^{0.2415}$

The functions were all within the 95% confidence interval and the r^2 values were all over 0.98.

Since the wind speed was larger in winter than in summer (Fig. 2a) and the duration of the northerly wind in winter was longer than that of the southerly wind in summer (Fig. 2b), the increasing concentration caused by the southerly wind in summer could not contend with the decreasing concentration caused by the northerly wind in winter, resulting in a lower C_a in case Control than in case No-wind throughout a year (Fig. 9c, d). On the other hand, wind-induced vertical mixing was also an important factor that facilitated vertical transport of contaminants and reduced C_a in case Control, especially in winter.

4.1.2. The role of air-sea heat flux

In case Constant-heat, C_v showed a high value in autumn and low value in spring, which were different from those in case Control (Fig. 9a). However, C_a showed a similar seasonal cycle with case Control though the value was a little lower in case Constant-heat than in case Control (Fig. 9c, d). It indicated that the vertical distribution of contaminant concentration in the water column, but not the surface value, was sensitive to seasonal variation in air-sea heat flux.

The annual mean air-sea heat flux used in case Constant-heat was shown in Supplementary Fig. 2. The waters inside the SIS gained heat, while the waters of the two boundaries, the Bungo Channel and Kii Channel, lost heat. In winter, the water temperature in case Constant-heat was higher in the middle area of the SIS than in two channels (Fig. 11a), which was opposite to the temperature distribution in case Control (Fig. 4a). The distributions of salinity were similar in the two cases (Fig. 4e and Fig. 11c). Determined by water temperature, density in case Constant-heat was low in the middle area and high in the two channels (Fig. 11e). The difference of density between middle area and two channels in case Constant-heat generated a horizontal pressure gradient force, inducing a surface density current toward the two channels and a deep density current toward the middle area, which could be addressed by the extension of isolines of temperature, salinity, and density (Fig. 11a, c, e).

In case Control, the density distribution was relatively uniform in winter (Supplementary Fig. 3a) and the horizontal current component due to density difference was weak (in principle, it is almost the same as the southward current of 0.7 cm/s in case No-wind, Fig. 10). The enhanced southward surface current in case Constant-heat (8.5 cm/s) (Fig. 10) brought more contaminants to the open ocean before they were vertically mixed within the water column. This can be known by vertically non-homogeneous distribution of concentration (Fig. 12a) and low concentration value in case Constant-heat (and Fig. 9a). As a result, continuous contaminant output to the open ocean from winter to spring (Fig. 10) contributed to the lowest C_v in spring (Figs. 9a and 12b).

In summer, there were similar density structures (Fig. 11f and Supplementary Fig. 3b) and meridional component of surface current velocity (Fig. 10) between case Control and case Constant-heat.

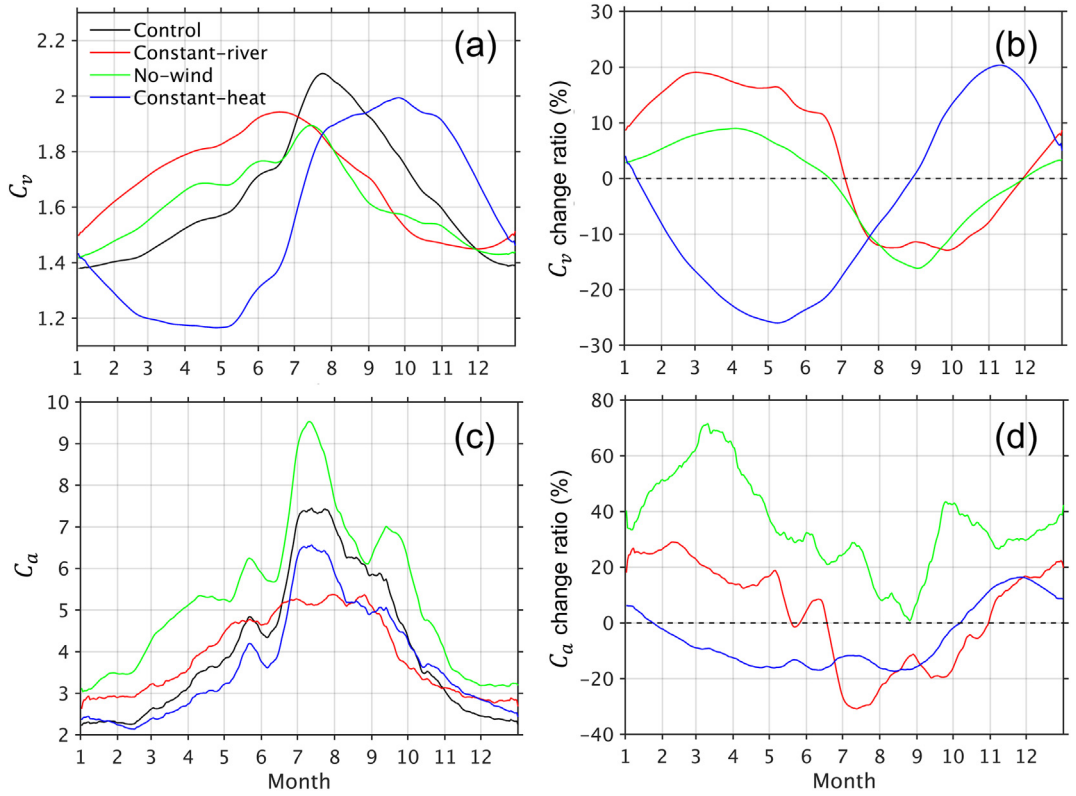

Fig. 9. Time series of 7-day running mean of (a) C_v in the numerical experiments and (b) their change ratios with respect to case Control. (c) and (d) are the same as (a) and (b), but for C_a.

However, a prominent change, i.e., the weakening of vertical stratification, was found in case Constant-heat in terms of the distributions of temperature (Figs. 4c and 11b), salinity (Figs. 4g and 11d), and density (Supplementary Fig. 3b and Fig. 11f). It was indicated that, in the condition of weak stratification, more contaminants entered the deep water since the water was vertically mixed more in case Constant-heat than in case Control (Figs. 7c and 12c). Contaminants in the deep water were easily accumulated from summer to autumn, resulting in the highest C_v in autumn (Figs. 9c and 12d).

4.1.3. The role of river discharge

Similar seasonal variations of contaminant concentration were shown in case Control and case Constant-river. However, the maximum concentration value became smaller in case Constant-river (red lines in Fig. 9a, c), especially for C_a in July that changed about 30% compared with case Control.

Change in river discharge had little impact on meridional component of sea surface current velocity over the entire SIS (Fig. 10); it mainly affected the amounts of contaminants entering the SIS. The integrated river water volume from daily river discharge used in case Control and case Constant-river were shown in Supplementary Fig. 4. The total river volume reached the same value in case Control and Constant-river in the middle of July, which was close to the time (early July) when the higher C_v in case Constant-river became lower than that in case Control (Fig. 9a). However, the inversion of C_a appeared in the middle of June (Fig. 9c), which was in accordance with the timing of drastic changes in river discharge (Fig. 2d). It was obvious that the surface concentration responded rapidly to the change in river discharge, not only response time but also concentration value indicated by higher change ratio of C_a than that of C_v between two cases (Fig. 9b, d).

As a summary, for C_v, the air-sea heat flux was the first contributor to its seasonal variability and concentration value, and river discharge was the secondary factor; for C_a, its seasonal variation was consistent

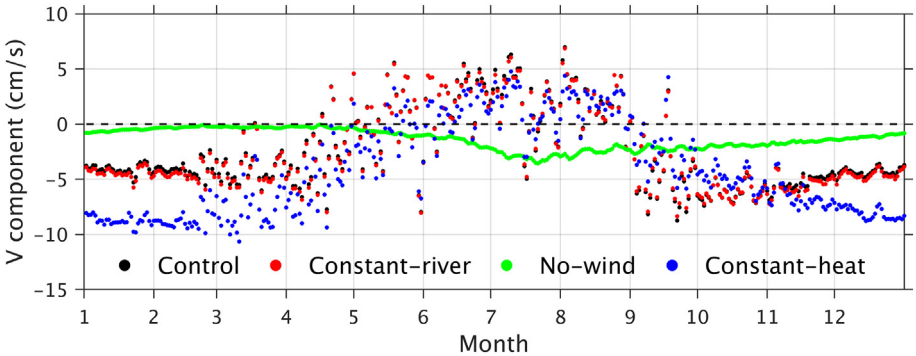

Fig. 10. Time series of the meridional component of surface current velocity averaged over the entire SIS in cases Control, Constant-river, No-wind, and Constant-heat. Northward current velocity is positive.

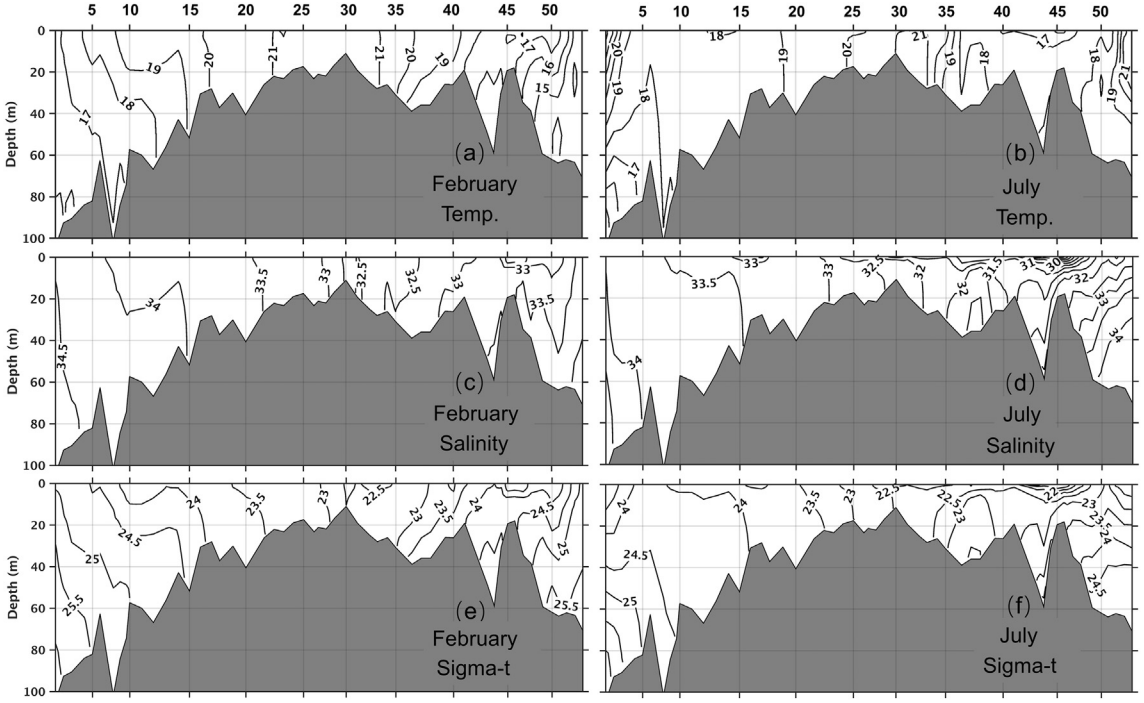

Fig. 11. Vertical distributions of (a–b) temperature (°C), (c–d) salinity, and (e–f) sigma-t (density-1000, kg/m^3) along the solid red line with numbers in Fig. 1c in February and July in case Constant-heat. (For interpretation of the references to colour in this figure legend, the reader is referred to the web version of this article.)

with that of river discharge, however, the sea surface wind velocity was the dominant factor controlling its value.

4.2. Comparison of dilution characteristics in wet and dry river years

Rivers act as the main source of contaminants in the SIS. With global climatic change in recent years, river discharge varies obviously and may have an important effect on contaminant concentration. Therefore, the responses of contaminant concentrations to river discharge need to be addressed. Supplementary Fig. 5a showed the long-term variations in annual mean river discharges of 26 rivers emptying into the SIS during 1993–2016 with a multi-year averaged value of 1010 m^3 s^{-1} and a standard deviation of 253 m^3 s^{-1}. Prominent dry year was observed in 1994 with an annual mean discharge of 536 m^3 s^{-1}, while prominent wet years were shown in 1993, 2004, 2015, and 2016 with an annual mean discharge around 1400 m^3 s^{-1}. Combined with case Control, two experiments named River-1994 and River-2015 were performed (Table 2) using river discharge in 1994 and 2015 (Table 1 and Supplementary Fig. 5b), which represented a dry river year and a wet river year, respectively, to investigate the impact of river discharge on contaminant concentration.

It was showed that the appearing time of maximum C_a were consistent with that of maximum river discharge (Supplementary Fig. 5b and Supplementary Fig. 6b). Moreover, C_v was high in March–June of 1994 and July of 1995 as a response to high river discharge at the same time (Supplementary Fig. 5b and Supplementary Fig. 6a). This indicated that high river discharge controlled the maximum contaminant concentration in both dry year and wet year of river.

When river discharge increased by 1.61 times (from 536 m^3 s^{-1} to 1400 m^3 s^{-1}), C_a increased by 1.55 times, while C_v increased by 1.33 times (Fig. 13a). It suggested that riverine contaminants tended to distribute in the surface layer. More specifically, when river discharge increased from 536 m^3 s^{-1} (case River-1994) to 1010 m^3 s^{-1} (case Control), the contaminant concentration increased in all sub-regions

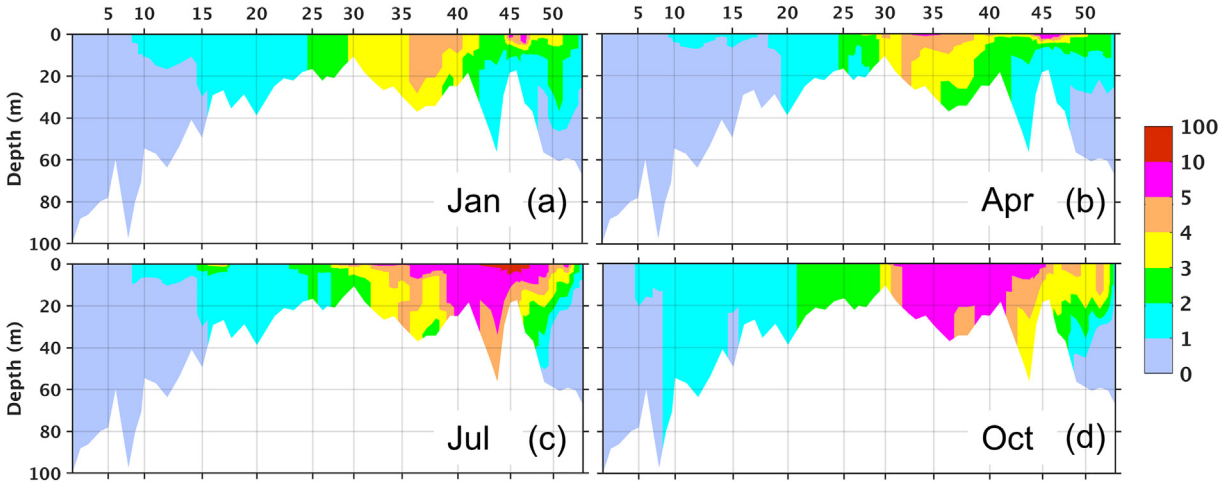

Fig. 12. The same as Fig. 7, but for case Constant-heat.

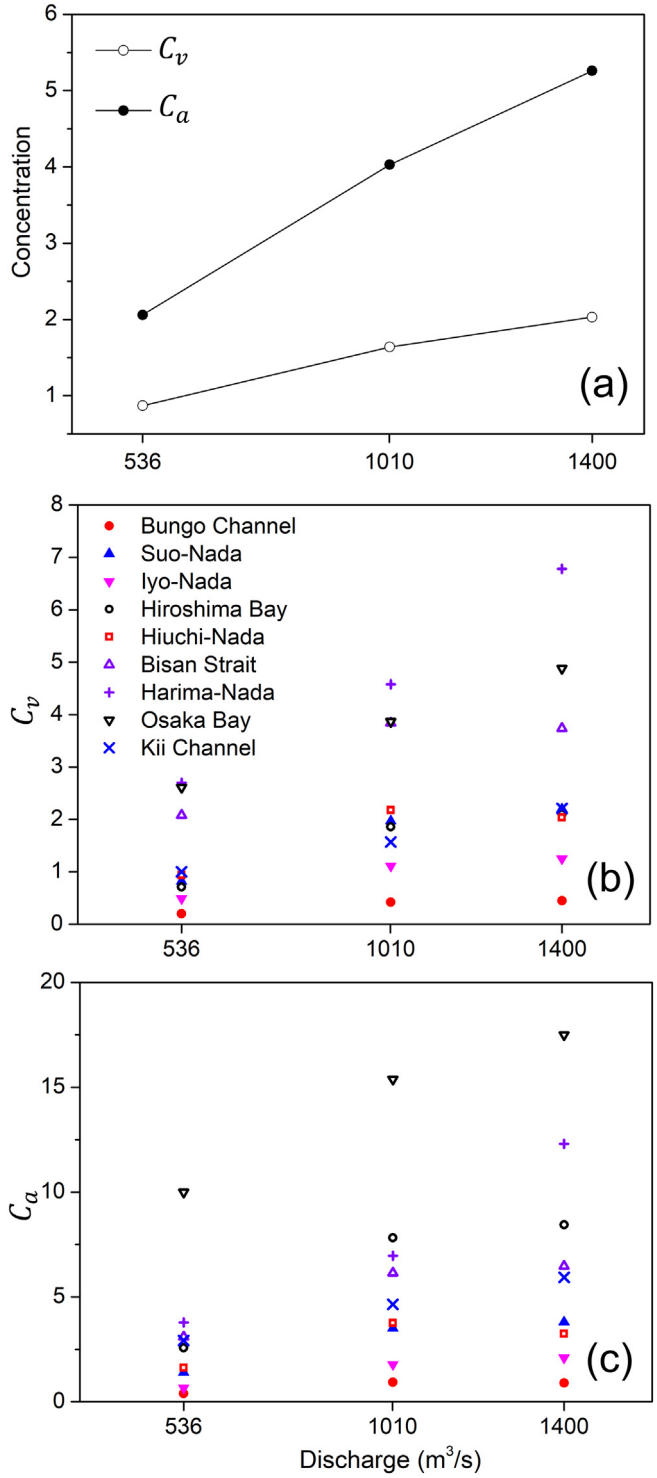

Fig. 13. The relationships between (a) contaminant concentration in the entire SIS and river discharge; (b) and (c) are the same but for C_v and C_a in several sub-regions of the SIS, respectively.

(Fig. 13b, c), which was in response to the increase in discharge of each river (Table 1).

However, when river discharge increased from 1010 $m^3 s^{-1}$ (case Control) to 1400 $m^3 s^{-1}$ (case River-2015), the responses of concentration were distinguishing in different sub-regions (Fig. 13b, c), which were related to the variations of river discharge (Table 1) near the sub-regions. A sharp increase in discharge of the Yodo River and Kako River (Table 1) caused obvious increasing of contaminant concentration in Osaka Bay and Harima-Nada. Slight increasing in Hiroshima Bay, Iyo-Nada and Suo-Nada were results of increasing discharges of rivers emptying into these sub-regions (Table 1). As pathways for contaminants flowing into open ocean, the concentrations in the Bungo Channel and Kii Channel increased as the same as adjacent sub-regions. On the contrary, a slight decreasing was denoted in the Bisan Strait and Hiuchi-Nada (Fig. 13b), which was caused by the combination (24.94 $m^3 s^{-1}$ reduction) of a reduction in discharge (43.41 $m^3 s^{-1}$) of Takahashi River and an increase in discharge (18.47 $m^3 s^{-1}$) of other four major rivers (the Yoshii River, Asahi River, Ashida River and Doki River) near the sub-regions (the discharge of secondary river in Hiuchi-Nada changed little).

This meant that the average contaminant concentration in the entire SIS was consistent with total river volume (Supplementary Figs. 4 and 6). However, the response of contaminant concentration in a sub-region corresponded to the variation of river discharge near this sub-region. This fact should be considered when evaluating and managing the riverine contaminant levels, such as nutrients, antibiotics, and other substances.

5. Conclusion

Based on a hydrodynamic model, this study investigated the dilution features of riverine input contaminants in the SIS. Conservative contaminant exhibited a vertically mixed pattern with low concentration in winter and a vertically varying pattern with high concentration in summer. High concentrations occurred in Osaka Bay, Harima-Nada, and Bisan Strait. With riverine input contaminant concentration of 100, the annual mean conservative contaminant concentrations were 1.64 and 4.03 for the water column and sea surface, respectively. Non-conservative contaminant showed a similar spatial distribution with the conservative contaminant. As the half-life period of non-conservative contaminant decreased, the contaminant concentration decreased following power functions. These were useful information for environmental management to set standards for contaminants to protect the health of the aquatic ecosystem of the SIS.

The roles played by surface wind velocity, air-sea heat flux and river discharge were confirmed with a series of numerical experiments. The seasonal cycle of air-sea heat flux was responsible for seasonal variations of contaminant concentrations in the whole water column by influencing horizontal current and vertical stratification. The surface wind velocity, which induced sea surface current, played a vital role affecting surface contaminant concentration. The appearing time of high contaminant concentration was always consistent with that of high river discharge. When river discharge increased from a dry river year to a wet river year, the contaminant concentration in the entire SIS increased but the concentrations in different sub-regions varied differently as a response to the change in river discharge near the sub-region. This should be considered when evaluating the level of contaminant concentration in different river years.

Once introduced into the sea surface water, except for decaying over time, the contaminants also undergo biodegradation and adsorption to suspended particles and sediment (Xu et al., 2009; Larcher and Yargeau, 2012; Ono et al., 2012). It should be noted that our hydrodynamic model did not include biological processes and adsorption to suspended particles or sediment that affect the behavior of contaminants. The impact of these processes will be investigated in future works.

Acknowledgement

This study was supported by the Ministry of Education, Culture, Sports, Science and Technology, Japan (MEXT) for a project by the Joint Usage/Research Center–Leading Academia in Marine and Environment Pollution Research (LaMer). X. Guo was also supported by JSPS KAKENHI Grant number JP17H01860. J. Zhu thanks the China

Scholarship Council (CSC) for supporting her stay in Japan.

Appendix A. Model description

The hydrodynamic model used in this study is based on the Princeton Ocean Model (Blumberg and Mellor, 1987), which is a three-dimensional free-surface primitive equation ocean model that has been widely applied to many coastal seas. Chang et al. (2009) used the three-dimensional numerical model with monthly forcing conditions to simulate the seasonal variation of sub-tidal current in the SIS. The model was updated with daily forcing conditions and applied in the present study. There were two southern boundaries in the model, Bungo Channel and Kii Channel (solid black lines in Fig. 1b). In fact, the SIS has another opening to the Tsushima Strait at its northwestern boundary, the Kanmon Strait (Fig. 1b). Since the Kanmon Strait is very narrow (approximately 0.6 km) and its influence on the SIS is small (Takeoka, 2002), it was closed in this model following previous studies (Takeoka, 1984; Kobayashi et al., 2006). The model had a horizontal resolution of 1/80° in the zonal direction and 1/120° in the meridional direction, and a vertical resolution of 21 sigma levels (0.000, −0.002, −0.004, −0.010, −0.020, −0.040, −0.060, −0.080, −0.100, −0.120, −0.140, −0.170, −0.200, −0.300, −0.400, −0.500, −0.650, −0.800, −0.900, −0.950, and −1.000). The internal mode time step was 120 s, and the external mode time step was 4 s.

The daily surface fluxes used to drive the model included surface fluxes of momentum, heat and fresh water. The daily wind stress was based on hourly averaged results of wind stress, which was calculated by wind velocity from the Grid Point Value of Meso-Scale Model (GPV-MSM) (http://database.rish.kyoto-u.ac.jp/arch/jmadata/data/gpv/) during 2007–2016 provided by the Japan Meteorological Agency with the resolution of 1/16° × 1/20°, adopting the drag coefficient of Large and Pond (1981). The northwest wind prevails in winter with an average speed of 4.3 m/s, while the southwest wind is dominant in summer with an average speed of 1.4 m/s (Fig. 2a, b). The daily shortwave radiation was based on the newly released of Japanese Ocean Flux Data Sets with Use of Remote Sensing Observation (J-OFURO3) (https://j-ofuro.scc.u-tokai.ac.jp/) with a resolution of 1/4° × 1/4° and averaged during 2002 to 2013. The daily longwave, sensible heat flux and latent heat flux were calculated and averaged by adopting bulk formula (Gill, 1982) using hourly air temperature, sea surface temperature, relative humidity, cloud cover, and wind velocity from the GPV-MSM (2007–2016). The SIS obtains around 131 W/m^2 of heat in summer and loses about 155 W/m^2 in winter (Fig. 2c). Daily evaporation was obtained by calculating the latent heat flux. The daily precipitation was provided by the GPV-MSM and averaged hourly from 2007 to 2016. Finally, the values of precipitation and evaporation were adjusted according to the values in Tawara (1986). The daily sea surface temperature was based on Operational Sea Surface Temperature and Sea Ice Analysis (OSTIA) (http://ghrsst-pp.metoffice.com/pages/latest_analysis/) with a resolution of 1/20° × 1/20° and averaged during 2007 to 2016. The sea surface temperature from OSTIA was adjusted by observed multi-year (1971 to 2000) monthly averaged sea surface temperature which was obtained from prefectural fishery research centers (dots in Fig. 1c).

The initial temperature and salinity fields in January were produced by merging the Marine Information Research Center dataset in the SIS region and the model results of Guo et al. (2003). The boundary conditions including de-tided current velocity, temperature, salinity, and surface elevation were obtained from the diagnostic model of Guo et al. (2004). There were four major tidal constituents, M_2, S_2, O_1 and K_1, along the open boundary provided by Matsumoto et al. (2000). The daily river discharges averaged over 24 years (1993–2016) from the Ministry of Land, Infrastructure and Transport were used in the model. Other detailed information about the model can be found in Chang et al. (2009).

A.1. Attenuation of non-conservative contaminant

The attenuation process of antibiotics is depicted by a first-order reaction kinetics model, in which the reaction rate is proportional to the reactant concentration. It follows that

$$\frac{dx}{dt} = -kx$$

where x is the reactant concentration, t is the reaction time, and k is the reaction rate constant. For a reactant concentration of x_0 at initial time t_0, the reactant concentration $x(t)$ at time t is

$$x(t) = x_0 e^{-k(t-t_0)}$$

In the model, the attenuation process of antibiotics is expressed by

$$x(t + \Delta t) = x(t) e^{-k \cdot \Delta t}$$

where $x(t)$ is the antibiotic concentration in the current time step, while $x(t + \Delta t)$ is the antibiotic concentration in the next time step, and Δt is the step time.

The half-life period is often used to show the persistence of antibiotics in the environment. In the first-order reaction kinetics model, the half-life period is independent of reactant concentration, but is inversely proportional to the reaction rate. If the half-life period is known as DT_{50}, the reaction rate constant k is $-\frac{\ln\left(\frac{1}{2}\right)}{DT_{50}}$. The half-life periods of OFL, RTM, ETM, and SMZ suggested by Xu et al. (2009) were used in the model.

Appendix A. Supplementary data

Supplementary data to this article can be found online at https://doi.org/10.1016/j.marpolbul.2019.02.029.

References

Baquero, F., Martínez, J.L., Cantón, R., 2008. Antibiotics and antibiotic resistance in water environments. Curr. Opin. Biotechnol. 19 (3), 260–265. https://doi.org/10.1016/j.copbio.2008.05.006.

Blumberg, A.F., Mellor, G.L., 1987. A description of a three-dimensional coastal ocean circulation model. In: Three-Dimensional Coastal Ocean Models. 4. pp. 1–16. https://doi.org/10.1029/CO004p0001.

Boon, P.I., Cattanach, M., 1999. Antibiotic resistance of native and faecal bacteria isolated from rivers, reservoirs and sewage treatment facilities in Victoria, south-eastern Australia. Lett. Appl. Microbiol. 28 (3), 164–168. https://doi.org/10.1046/j.1365-

2672.1999.00517.x.
Burreau, S., Zebühr, Y., Broman, D., Ishaq, R., 2006. Biomagnification of PBDEs and PCBs in food webs from the Baltic Sea and the northern Atlantic Ocean. Sci. Total Environ. 366 (2–3), 659–672. https://doi.org/10.1016/j.scitotenv.2006.02.005.
Chang, P.H., Guo, X., Takeoka, H., 2009. A numerical study of the seasonal circulation in the Seto Inland Sea, Japan. J. Oceanogr. 65 (6), 721.
Chow, L., Waldron, L., Gillings, M.R., 2015. Potential impacts of aquatic pollutants: sub-clinical antibiotic concentrations induce genome changes and promote antibiotic resistance. Front. Microbiol. 6, 803. https://doi.org/10.3389/fmicb.2015.00803.
da Silva, B.F., Jelic, A., López-Serna, R., Mozeto, A.A., Petrovic, M., Barceló, D., 2011. Occurrence and distribution of pharmaceuticals in surface water, suspended solids and sediments of the Ebro river basin, Spain. Chemosphere 85 (8), 1331–1339. https://doi.org/10.1016/j.chemosphere.2011.07.051.
Gill, A.E., 1982. Atmosphere-Ocean Dynamics. Academic Press.
Gómez-Gutiérrez, A., Garnacho, E., Bayona, J.M., Albaigés, J., 2007. Screening ecological risk assessment of persistent organic pollutants in Mediterranean sea sediments. Environ. Int. 33 (7), 867–876. https://doi.org/10.1016/j.envint.2007.04.002.
Grill, G., Khan, U., Lehner, B., Nicell, J., Ariwi, J., 2016. Risk assessment of down-the-drain chemicals at large spatial scales: model development and application to contaminants originating from urban areas in the Saint Lawrence River Basin. Sci. Total Environ. 541, 825–838. https://doi.org/10.1016/j.scitotenv.2015.09.100.
Guo, X., Hukuda, H., Miyazawa, Y., Yamagata, T., 2003. A triply nested ocean model for simulating the Kuroshio—roles of horizontal resolution on JEBAR. J. Phys. Oceanogr. 33 (1), 146–169. https://doi.org/10.1175/1520-0485(2003)033<0146:ATNOMF>2.0.CO;2.
Guo, X., Futamura, A., Takeoka, H., 2004. Residual currents in a semi-enclosed bay of the Seto Inland Sea, Japan. J. Geophys. Res. Oceans 109 (C12). https://doi.org/10.1029/2003JC002203.
Halling-Sørensen, B., Nielsen, S.N., Lanzky, P.F., Ingerslev, F., Lützhøft, H.H., Jørgensen, S., 1998. Occurrence, fate and effects of pharmaceutical substances in the environment-a review. Chemosphere. 36 (2), 357–393. https://doi.org/10.1016/S0045-6535(97)00354-8.
Hanawa, K., Mitsudera, H., 1985. On daily average of oceanographic data (in Japanese). Coast. Oceanogr. Bull. 23, 79–87.
Hirsch, R., Ternes, T., Haberer, K., Kratz, K.L., 1999. Occurrence of antibiotics in the aquatic environment. Sci. Total Environ. 225 (1–2), 109–118. https://doi.org/10.1016/S0048-9697(98)00337-4.
Hu, L., Zhang, G., Zheng, B., Qin, Y., Lin, T., Guo, Z., 2009. Occurrence and distribution of organochlorine pesticides (OCPs) in surface sediments of the Bohai Sea, China. Chemosphere 77 (5), 663–672. https://doi.org/10.1016/j.chemosphere.2009.07.070.
Iwata, H., Tanabe, S., Sakai, N., Tatsukawa, R., 1993. Distribution of persistent organochlorines in the oceanic air and surface seawater and the role of ocean on their global transport and fate. Environ. Sci. Technol. 27 (6), 1080–1098.
Karunasagar, I., Pai, R., Malathi, G.R., Karunasagar, I., 1994. Mass mortality of Penaeus monodon larvae due to antibiotic-resistant Vibrio harveyi infection. Aquaculture 128 (3–4), 203–209. https://doi.org/10.1016/0044-8486(94)90309-3.
Kobayashi, S., Simpson, J.H., Fujiwara, T., Horsburgh, K.J., 2006. Tidal stirring and its impact on water column stability and property distributions in a semi-enclosed shelf sea (Seto Inland Sea, Japan). Cont. Shelf Res. 26 (11), 1295–1306. https://doi.org/10.1016/j.csr.2006.04.006.
Larcher, S., Yargeau, V., 2012. Biodegradation of sulfamethoxazole: current knowledge and perspectives. Appl. Microbiol. Biotechnol. 96 (2), 309–318.
Large, W.G., Pond, S., 1981. Open ocean momentum flux measurements in moderate to strong winds. J. Phys. Oceanogr. 11 (3), 324–336. https://doi.org/10.1175/1520-0485(1981)011<0324:OOMFMI>2.0.CO;2.
Lee, Y.J., Lee, S.E., Lee, D.S., Kim, Y.H., 2008. Risk assessment of human antibiotics in Korean aquatic environment. Environ. Toxicol. Pharmacol. 26 (2), 216–221. https://doi.org/10.1016/j.etap.2008.03.014.
Liu, S., Zhao, H., Lehmler, H.J., Cai, X., Chen, J., 2017. Antibiotic pollution in marine food webs in Laizhou Bay, North China: trophodynamics and human exposure implication. Environ. Sci. Technol. 51 (4), 2392–2400.
Liu, L., Wu, W., Zhang, J., Lv, P., Xu, L., Yan, Y., 2018. Progress of research on the toxicology of antibiotic pollution in aquatic organisms. Acta Ecol. Sin. 38 (1), 36–41. https://doi.org/10.1016/j.chnaes.2018.01.006.
Lohmann, R., Jurado, E., Pilson, M.E., Dachs, J., 2006. Oceanic deep water formation as a sink of persistent organic pollutants. Geophys. Res. Lett. 33 (12). https://doi.org/10.1029/2006GL025953.
Majtán, J., Černy, J., Ofúkaná, A., Takáč, P., Kozánek, M., 2012. Mortality of therapeutic fish Garra rufa caused by Aeromonas sobria. Asian Pac. J. Trop. Biomed. 2 (2), 85.
Managaki, S., Murata, A., Takada, H., Tuyen, B.C., Chiem, N.H., 2007. Distribution of macrolides, sulfonamides, and trimethoprim in tropical waters: ubiquitous occurrence of veterinary antibiotics in the Mekong Delta. Environ. Sci. Technol. 41 (23), 8004–8010. https://doi.org/10.1021/es0709021.
Marti, E., Variatza, E., Balcazar, J.L., 2014. The role of aquatic ecosystems as reservoirs of antibiotic resistance. Trends Microbiol. 22 (1), 36–41. https://doi.org/10.1016/j.tim.2013.11.001.
Matsumoto, K., Takanezawa, T., Ooe, M., 2000. Ocean tide models developed by assimilating TOPEX/POSEIDON altimeter data into hydrodynamical model: a global model and a regional model around Japan. J. Oceanogr. 56 (5), 567–581.
Minh, T.B., Leung, H.W., Loi, I.H., Chan, W.H., So, M.K., Mao, J.Q., Choi, D., Lam, J.C.W., Zheng, G., Martin, M., Lee, J.H.W., Lam, P.K.S., Richardson, B.J., 2009. Antibiotics in the Hong Kong metropolitan area: ubiquitous distribution and fate in Victoria Harbour. Mar. Pollut. Bull. 58 (7), 1052–1062. https://doi.org/10.1016/j.marpolbul.2009.02.004.
Montuori, P., Triassi, M., 2012. Polycyclic aromatic hydrocarbons loads into the Mediterranean Sea: estimate of Sarno River inputs. Mar. Pollut. Bull. 64 (3), 512–520. https://doi.org/10.1016/j.marpolbul.2012.01.003.
Murata, A., Takada, H., Mutoh, K., Hosoda, H., Harada, A., Nakada, N., 2011. Nationwide monitoring of selected antibiotics: distribution and sources of sulfonamides, trimethoprim, and macrolides in Japanese rivers. Sci. Total Environ. 409 (24), 5305–5312. https://doi.org/10.1016/j.scitotenv.2011.09.014.
Nagai, T., 2003. Recovery of fish stocks in the Seto Inland Sea. Mar. Pollut. Bull. 47 (1–6), 126–131. https://doi.org/10.1016/S0025-326X(03)00100-0.
Ono, J., Takahashi, D., Guo, X., Takahashi, S., Takeoka, H., 2012. A numerical study on the seasonal variability of polychlorinated biphenyls from the atmosphere in the East China Sea. Chemosphere. 89 (4), 389–397. https://doi.org/10.1016/j.chemosphere.2012.05.049.
Takeoka, H., 1984. Exchange and transport time scales in the Seto Inland Sea. Cont. Shelf Res. 3 (4), 327–341. https://doi.org/10.1016/0278-4343(84)90015-3.
Takeoka, H., 2002. Progress in Seto Inland Sea research. J. Oceanogr. 58 (1), 93–107.
Tawara, S., 1986. Studies on the characteristic of oceanographic condition in relation to fishing condition in the shallow coastal waters. J. Shimonoseki Univ. Fish. 34 (1), 1–103.
Vivekanandhan, G., Savithamani, K., Hatha, A.A.M., Lakshmanaperumalsamy, P., 2002. Antibiotic resistance of Aeromonas hydrophila isolated from marketed fish and prawn of South India. Int. J. Food Microbiol. 76 (1–2), 165–168. https://doi.org/10.1016/S0168-1605(02)00009-0.
Wang, H., Guo, X., Liu, Z., 2019. The age of Yodo River water in the Seto Inland Sea. J. Mar. Syst. 191, 24–37. https://doi.org/10.1016/j.jmarsys.2018.12.001.
Wolschke, H., Xie, Z., Möller, A., Sturm, R., Ebinghaus, R., 2011. Occurrence, distribution and fluxes of benzotriazoles along the German large river basins into the North Sea. Water Res. 45 (18), 6259–6266. https://doi.org/10.1016/j.watres.2011.09.028.
Xu, W.H., Zhang, G., Zou, S.C., Li, X.D., Liu, Y.C., 2007. Determination of selected antibiotics in the Victoria Harbour and the Pearl River, South China using high-performance liquid chromatography-electrospray ionization tandem mass spectrometry. Environ. Pollut. 145 (3), 672–679. https://doi.org/10.1016/j.envpol.2006.05.038.
Xu, W.H., Zhang, G., Wai, O.W., Zou, S.C., Li, X.D., 2009. Transport and adsorption of antibiotics by marine sediments in a dynamic environment. J. Soils Sediments 9 (4), 364–373.
Yanagi, T., 1981. In: Tide and tidal current in the Seto Inland Sea. In Proc. 28th Conf. Coast. Eng., JSCE. pp. 555–558.
Yanagi, T., Takeoka, H., Tsukamoto, H., 1982. Tidal energy balance in the Seto Inland Sea. J. Oceanogr. Soc. Jpn 38 (5), 293–299.
Zhang, R., Zhang, G., Zheng, Q., Tang, J., Chen, Y., Xu, W., Zou, Y., Chen, X., 2012. Occurrence and risks of antibiotics in the Laizhou Bay, China: impacts of river discharge. Ecotoxicol. Environ. Saf. 80, 208–215. https://doi.org/10.1016/j.ecoenv.2012.03.002.
Zhao, J.L., Ying, G.G., Liu, Y.S., Chen, F., Yang, J.F., Wang, L., Yang, X.B., Stauber, J.L., Warne, M.S.J., 2010. Occurrence and a screening-level risk assessment of human pharmaceuticals in the Pearl River system, South China. Environ. Toxicol. Chem. 29 (6), 1377–1384. https://doi.org/10.1002/etc.161.
Zou, S., Xu, W., Zhang, R., Tang, J., Chen, Y., Zhang, G., 2011. Occurrence and distribution of antibiotics in coastal water of the Bohai Bay, China: impacts of river discharge and aquaculture activities. Environ. Pollut. 159 (10), 2913–2920. https://doi.org/10.1016/j.envpol.2011.04.037.